

Impact of Eddy-Induced Transport on the Lagrangian Structure of the Upper Branch of the Thermohaline Circulation

S. S. DRIJFHOUT AND P. DE VRIES

Royal Netherlands Meteorological Institute (KNMI), De Bilt, Netherlands

K. DÖÖS

Department of Meteorology, Stockholm University, Stockholm, Sweden

A. C. COWARD

Southampton Oceanography Centre, Southampton, United Kingdom

(Manuscript received 14 February 2002, in final form 26 March 2003)

ABSTRACT

The effect of the eddy-induced transport (EIT) on the Lagrangian structure of the upper branch of the thermohaline circulation is investigated. The Lagrangian pathways, transport, and flow characteristics such as the large-scale chaotic mixing are examined in the OCCAM global, eddy-permitting ocean general circulation model. The motions of water masses are traced employing Lagrangian trajectories. These are computed using both the time-averaged Eulerian velocity and a velocity field that contains the EIT. In all aspects of the flow investigated the neglect of the EIT leads to severely biased results. Below the mixed layer divergences of eddy mass fluxes nearly cancel those of the mean flow. As a result, diapycnal motion is reduced by the EIT. In the surface layer, the EIT counteracts the Ekman flow. This compensation is found to hold both locally and nearly everywhere in the basin. Typically, the surface layer EIT reduces the Ekman transport by 50%. Both reduced diapycnal motion and compensation of the Ekman flow prolong the circulation in wind-driven gyres and counteract dispersion of particles into the interior. Subsequently, the distribution of Lagrangian transport times becomes more peaked at shorter timescales and the transport times between sections decrease. At longer timescales the functional time dependence of the distribution is significantly changed. The spreading of particles and water masses without the EIT is governed by the “wrong” physics. The fact that the EIT makes the flow more aligned along isopycnals, and subsequently more quasi two-dimensional, implies reduced chaotic mixing.

1. Introduction

Until recently, the formation and distribution of the global-scale water masses and the associated thermohaline circulation (THC) has been studied by relying both on restricted observational datasets and coarse-resolution ocean general circulation models (OGCMs) (e.g., England 1993; Drijfhout et al. 1996). The motivating factors for the use of coarse-resolution OGCMs, apart from computational efficiency, are the observations that the characteristic spatial scales of the THC are large in comparison with the internal Rossby radius and that its characteristic timescales are large in comparison with the typical periods of the mesoscale eddy field. This approach assumes tacitly that the large-scale THC is not critically influenced by smaller-scale

details of the flow, such as the structure of boundary currents, equatorial currents, currents in passages, upwelling regimes, and so on. Also, eddies are assumed not to rectify the Eulerian mean flow on these large scales, or to affect the global-scale water mass transports.

These assumptions are questionable. They are partially motivated by the necessity for relying on coarse-resolution models when an equilibrium is to be achieved within the time integration. The alternative of using a higher-resolution ocean model that resolves more of the relevant details of the flow implies an integration of at most a few decades, leaving a large-scale drift in the deep water masses. From such higher-resolution simulations we learn that the THC and wind-driven circulation interact extensively, most noticeably in the upper ocean and Antarctic Circumpolar Current (ACC) and that eddies play an important role in this interaction (e.g., Semtner and Chervin 1992; Döös 1995). To isolate the effect of eddies, integrations of a high-resolution

Corresponding author address: S. S. Drijfhout, Royal Netherlands Meteorological Institute (KNMI), P.O. Box 201, 3730 AE De Bilt, Netherlands.
E-mail: drijfhou@knmi.nl

and coarse-resolution version of the same model can be compared (Thompson et al. 1997). This isolation is, however, never clear-cut. The effect of the eddies cannot be separated from those that result from a change in resolution, diffusion, and viscosity parameters.

One aspect of the eddy field that can be exactly calculated is the eddy-induced transport (EIT) of tracers and water masses. In eddy-resolving/permitting models it can be calculated by subtracting from the time-averaged isopycnal mass transport the mass transport due to the time-mean flow (see Hazeleger et al. 2003). The difference between the two, the EIT, results from the correlations between velocity and isopycnal thickness variations. In coarse-resolution models, the EIT can be included in parameterized form. Using the Gent and McWilliams (1990; GM) parameterization, Danabasoglu and McWilliams (1995) found significant changes in the global-scale circulation, most noticeably a cancellation of the Deacon cell. The same cancellation occurs in high-resolution models without the GM parameterization (Döös and Webb 1994). It was also found that the EIT counteracts the Ekman transport and its deeper return flow in tropical wind-driven cells (Hazeleger et al. 2001) and at midlatitudes (Bryan 1986; Drijfhout 1994a). So, away from the Southern Ocean, the EIT seems most important above the thermocline where the THC and wind-driven circulations interact.

In the present study, the effect of the EIT on the upper branch of the THC will be elucidated by tracing the motion of water masses employing Lagrangian trajectories. The latter are calculated using both the time-averaged Eulerian mean velocity field and a velocity field that contains the (time independent) EIT. The EIT is diagnosed from a series of 5-day running means from the global high-resolution ocean model OCCAM (Webb et al. 1997). A quantitative picture of the three-dimensional water movement associated with the upper branch of the THC is obtained, as well as the change in this circulation due to the EIT. The effects of the EIT are quite general but can be most easily demonstrated in the upper-layer flows where they are prominent. In the Southern Ocean the effect of eddies on the deep circulation can be complicated and possibly far reaching (Toggweiler and Samuels 1995; Gnanadesikan 1999). In addition, we discuss the results within the context of previous theories on eddy-mean flow interaction with special emphasis on the role of eddy transports in supplying the Ekman flow.

The 3D Lagrangian structure of the global conveyor belt has been analyzed before by, for example, Döös (1995), Drijfhout et al. (1996), Döös and Coward (1997), and Speich et al. (2001), but the effect of the EIT has not been explicitly addressed in this context. The impact of the EIT on the Lagrangian structure of the upper branch of the THC is also described with diagnostics used in studies on chaotic mixing. An analysis of the Lagrangian structure of the time-averaged THC in terms of chaotic behavior and dynamical sys-

tems theory has been attempted by, for example, Yang and Liu (1997) and Nycander et al. (2002). Apart from the seasonal cycle, the flow we study is time independent. Many aspects of chaotic advection are therefore absent in the velocity fields considered. A 3D time-averaged flow, however, also gives rise to chaos (Yang and Liu 1997).

This paper is organized as follows. In section 2 we discuss the model and Lagrangian methodology. In section 3 the impact of the EIT on flow pathways is presented in terms of horizontal transport streamfunctions. Also, the impact of the EIT on diapycnal transport and implied watermass conversion is discussed. A theoretical discussion on the eddy-induced changes is given in section 4. Section 5 presents the spread and mixing of particles and the distribution of Lagrangian timescales. In section 6 we summarize and present our conclusions.

2. Methodology

Data have been employed from model years 9.0 to 12.0 of the OCCAM integration. The model has 36 levels in the vertical and a uniform horizontal resolution of $\frac{1}{4}^\circ$ by $\frac{1}{4}^\circ$. The wind forcing was defined from 6-hourly European Centre for Medium-Range Weather Forecasts (ECMWF) winds. Years 9.0 to 12.0 of the model use wind stresses from 1993 to 1995 inclusive. Buoyancy fluxes were derived from relaxing the sea surface temperature and salinity to the Levitus 1994 climatology. A model climatology was constructed from 219 archived 5-day averages. We calculate the mean velocity field over the 3-yr period and use this as, apart from the seasonal cycle, a time-invariant field when calculating offline Lagrangian trajectories. The velocity field is still close to a diagnostic calculation of the Levitus 1994 climatology. An added value to a diagnostic calculation as obtained from inverse models (e.g., McDonald and Wunsch 1996) is that a short run of the high-resolution model has effectively interpolated the smoothed climatology on a high-resolution grid in a dynamically consistent manner, introducing realistic boundary currents and fronts (Saunders et al. 1999). Another advantage is that the model fields are hardly constrained by the poorly known surface buoyancy fluxes and by the even less well established interior diapycnal mixing coefficient. The disadvantage is that the velocities are affected by model drift. Model drift acts as a spurious source for diapycnal motion in Lagrangian calculations. It is not trivial to isolate the effect of drift on the velocity fields and to correct for it. As a result, we have not made any attempt to do this. The velocity fields contain more diapycnal motion than would be present in the absence of drift. By comparing trajectories from calculations with and without EIT, the largest part of the effect of drift is eliminated, assuming that drift is largest in the mean fields. Moreover, we focus on the upper branch of the THC while the largest drift occurs

in the deeper layers. The impact of drift on the calculations is further discussed in the next section.

The EIT is calculated from the correlations between velocity and isopycnal thickness variations. This has been done by transforming the 5-day-averaged velocities from z to density (σ_0) coordinates, determining the time-averaged isopycnal mass transport, and finally transforming this quantity back to z coordinates. We discriminate for the season in the averaging procedure. In this way, a velocity field is obtained that contains both the seasonal-mean component as well as the eddy-induced component. For more details on this calculation we refer to Hazeleger et al. (2003).

The tracing technique used here was originally developed by Döös (1995) and Blanke and Raynaud (1997). For a given velocity field the trajectories are analytically solved within each grid cell. This method allows the calculation of thousands to millions of trajectories for very long periods (de Vries and Döös 2001). Following Döös (1995), a fixed transport is associated to each trajectory. As a consequence, the particle seeding at the initial section is proportional to the cross-sectional transport in each grid box. In most applications, results converge when we associate a transport of about 10^{-3} Sv ($\text{Sv} \equiv 10^6 \text{ m}^3 \text{ s}^{-1}$) to each particle. This implies about 15 000 particles to trace the THC. From the individual trajectories a Lagrangian transport streamfunction can be constructed between arbitrary sections for any water mass or flow contained within a certain density class and flowing between those two sections (Blanke and Raynaud 1997).

A time-dependent trajectory algorithm has been used with time interpolation between seasonally varying velocity fields. In principle, a time-independent trajectory algorithm can also be used. In which case, the particle is always advected with the initial velocities at each Lagrangian integration step (e.g., Speich et al. 2001). We have compared results that are obtained with this method with results obtained by using the more expensive (a factor of 2–3) time-dependent trajectory algorithm of de Vries and Döös (2001). The error due to incorrect time interpolation was generally in between 0 and 20%, which we considered too large. Therefore, the computations with the seasonally varying fields were performed by using the time-dependent trajectory algorithm of de Vries and Döös (2001). To retain a correct mean seasonal cycle all seasonally varying fields were interpolated according to the method of Killworth (1996). Our tracing method gives similar results as “conventional” methods using a time-stepping technique. The method used here gives an exact analytical solution for the trajectory in each grid box. For more discussion on the differences between this tracing technique and previous ones we refer to de Vries and Döös (2001). An important element in our study is that a fixed transport is associated with each particle. As a result, our Lagrangian calculations can be made quantitative, while previous ones were often qualitative. This partic-

ular seeding technique does not rely on the tracing method used and could also be applied to other tracing methods.

3. The Lagrangian trajectories

Eddies will spread out trajectories by turbulent isopycnal mixing that is associated with the time dependence of the flow. We will not address this aspect of the eddy field. To resolve the time variability of the eddy field on a global domain requires computer resources that are unavailable at present. On the other hand, eddies do have a time-mean effect on the circulation. One effect is the rectification of the mean flow. To address this, two simulations of a fine- and a coarse-resolution version of the same model would be needed with all other parameters fixed. Such a twin experiment has not been performed with the present model. A second effect of the eddies on the time-mean flow results from the correlations between density, or layer thickness, and velocity. Because of this correlation, the eddies contribute to the time-averaged mass transports and eddy transports must be included in the calculation of a true streamfunction in density space. To account for the eddy transports in Eulerian space, a bolus velocity, $\mathbf{u}^* = (u^*, v^*)$, has to be added to the time-mean flow $\bar{\mathbf{u}} = (\bar{u}, \bar{v})$, where the bar denotes a time average. On isopycnals the bolus velocity can be expressed as

$$\mathbf{u}^*(\sigma) = \frac{\overline{\mathbf{u}'(\sigma)h'(\sigma)/h(\sigma)}}, \quad (1)$$

where the prime, h and σ denote deviations from the time-averaged layer thickness and density, respectively. In the remainder we will discuss the impact of \mathbf{u}^* (or the EIT $\equiv \mathbf{u}^*h$) on the steady 3D ocean circulation. In many cases we allow the flow to vary slowly in order to capture the seasonal cycle. This type of slowly evolving time variation does not qualitatively alter the Lagrangian structure of the flow. When discussing the results we assume for simplicity that the flow is time independent.

a. Pathways

Following Speich et al. (2001) the upper branch of the THC was backtraced from the Atlantic equator to the boundaries of the Indian–Atlantic basin. The northward flow at the Atlantic equator in density classes lighter than $\sigma_0 = 27.6$ was seeded with particles resolving $1000 \text{ m}^3 \text{ s}^{-1}$ volume transport each. The Lagrangian transport streamfunction has been calculated from the transports associated with the trajectories that together define the upper branch of the THC. Particles were advected by seasonal-mean velocities with and without the EIT. The results are shown in Fig. 1. The streamfunctions are calculated by defining zero values at the African continent. In this way, at the Atlantic equator the streamfunction equals the, from east to west, zonally integrated northward transport. There appear to be three

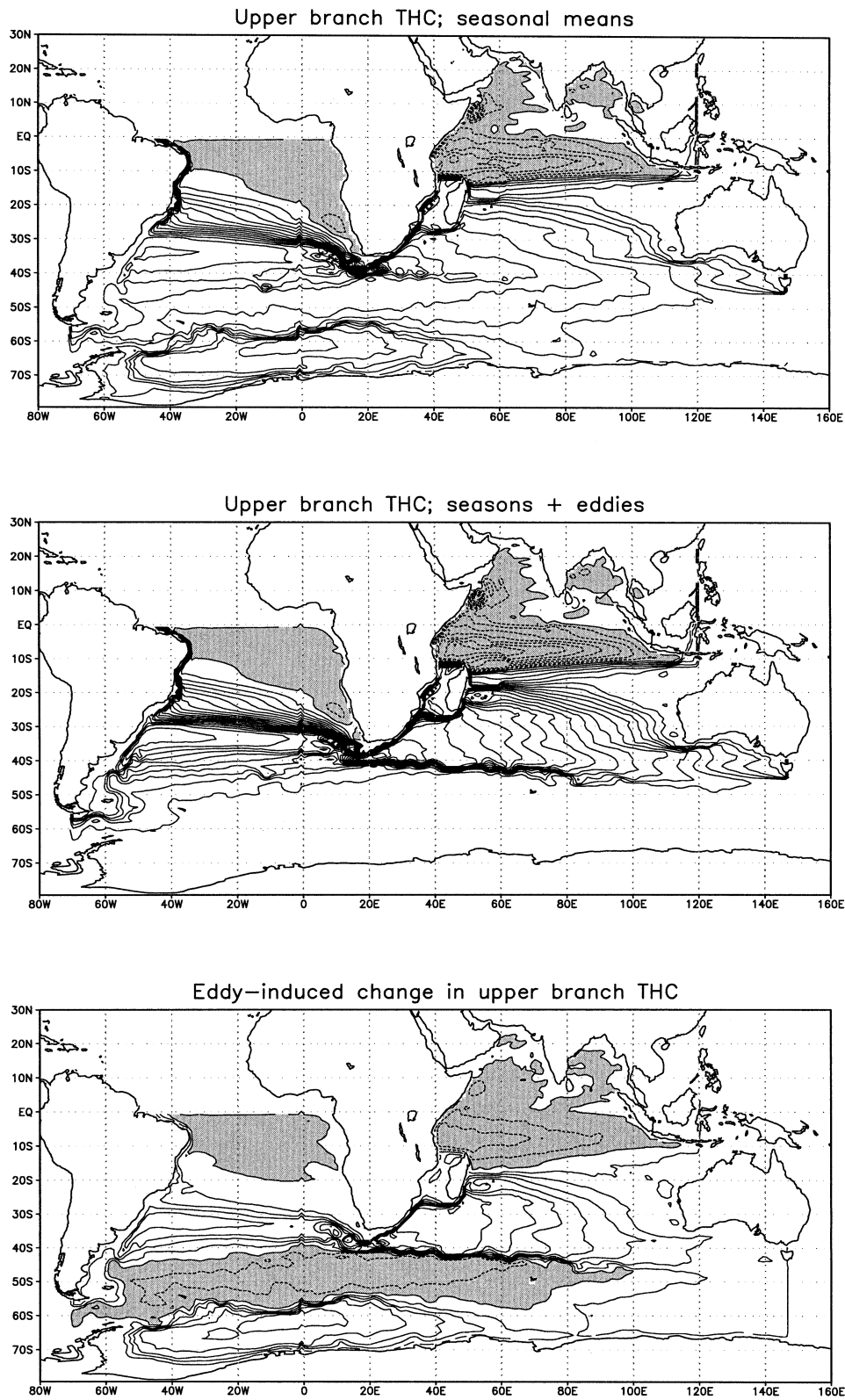


FIG. 1. Lagrangian horizontal streamfunction of the vertically integrated transport of the upper branch of the THC between the Indian–Atlantic borders and the Atlantic equator. The contour interval is 1 Sv ($\equiv 10^6 \text{ m}^3 \text{ s}^{-1}$). With each particle a transport of about $1000 \text{ m}^3 \text{ s}^{-1}$ is associated. The streamfunction is calculated by defining zero values at the African continent. Regions with negative values are gray, denoting recirculations that oppose the direct pathways of the THC. Negative contours are stippled.

pathways from the Pacific to the Atlantic. One originates from Drake Passage. The other two pass through the Indian Ocean. Eastward from 90°E a bifurcation occurs. Part of the flow comes from the south of Australia. This flow has been coined “Tasman leakage,” and was described by Speich et al. (2002). The other part comes from the Indonesian Throughflow. The eddy-induced changes in the pathways involve increased recirculation in the wind-driven gyres and a strong signal in the Southern Ocean, south of 40°S and between 60°W and 40°E. To better understand this, the eddy-induced change for each route is shown in Fig. 2.

The results obtained without the EIT show that part of the flow is trapped into a clockwise recirculation south of the ACC. This recirculation mainly occurs at density levels below $\sigma_0 = 27.4$. Also, the eastward flow in the South Atlantic occurs farther to the south and is distributed over the whole ACC. When the EIT is included, the following differences are evident: The return flow, originating from Drake Passage, is more concentrated in the Malvinas Current. The eastward flow in the South Atlantic occurs farther to the north and is more concentrated in the South Atlantic Current. The eastward flow south of 40°S is almost absent and the flow is no longer trapped in the recirculation south of the ACC. The Indian and South Atlantic supergyre recirculation (de Ruijter 1982) is narrowed by the EIT. Furthermore, recirculation in the subtropical gyre of the Indian Ocean increases for flow originating from the Indonesian Throughflow. Also, clockwise recirculation in the tropical Indian Ocean between the South Equatorial Current and the Equatorial Undercurrent is increased. With the EIT the flow remains more in the lighter density classes. Without it the along-trajectory density changes are much larger. As a result, gyre-scale recirculation in the upper ocean is increased, while wide (and long) recirculations with larger vertical scale decrease. The travel path and travel time between different sections are subsequently shortened.

The result that the EIT focuses the flow in recirculations associated with western boundary currents and midlatitude jets implies that it does not act in a diffusive manner on the momentum and mass transport. Instead, an upgradient momentum transfer occurs in the wind-driven gyres, at least in the western part where the circulation is strongest. The flow from the south of Australia occurs on deeper levels than the flow from the other origins. As a result, the typical wind-driven recirculations are weak. Even so, the effect of the EIT in focusing the flow into gyre-scale recirculations is also demonstrated for this route. The wide Indian–Atlantic supergyre recirculation and the clockwise recirculation poleward of the ACC are almost absent when the EIT is included.

The Lagrangian streamfunction for the flow originating from Drake Passage seems more affected by the EIT than the streamfunctions for the flow from the other two origins. This suggests that the EIT plays a more

prominent role in the Southern Ocean than in the subtropical and tropical basins. This also corroborates the earlier finding that the most conspicuous effect of the EIT is compensating the Eulerian mean flow associated with the Deacon cell (Hirst and McDougall 1998).

b. Diapycnal motion

The impact of EIT on the pathways of the upper branch of the THC strongly suggests that the along-trajectory density change is reduced. As a result, the EIT constrains the flow to be more along isopycnals with diminishing diapycnal motion. To test this we repeated the former calculation with increased particle resolution ($250 \text{ m}^3 \text{ s}^{-1}$ volume transport) to monitor the various upwelling and downwelling events across several density surfaces. Below the surface mixed layer upwelling and downwelling is diminished by the EIT. This effect becomes stronger when the respective density surface is found at greater depth. We restrict ourselves to flow above the $\sigma_0 = 27.6$ surface, so the deepest density surfaces we consider are still found at mid-depth. A most striking example (Fig. 3) is given by the upwelling across the $\sigma_0 = 27.4$ surface. Without the EIT 4.5 Sv of water, still denser than $\sigma_0 = 27.4$ at the boundaries of the Indian–Atlantic basin, upwells into lighter density classes while flowing toward the Atlantic equator. With the EIT this amount is reduced to 1.0 Sv (Fig. 3). Water coming from the Indonesian Throughflow generally subducts along its path and gains density while transecting the Indian Ocean. Water coming from the south of Australia and Drake Passage upwells. The unventilated water coming from Drake Passage and the south of Australia on average upwell from 960 to 500 m at the Atlantic equator when the EIT is not accounted for. With the EIT the upwelling is only from 630 to 500 m. The implied density loss in σ_0 units is 0.27 versus 0.05, respectively. It can be concluded that EIT counteracts subsurface diapycnal excursions as well as entrainment into the mixed layer.

It has been found that introducing eddies into a level coordinate model results in excess water mass transformation (Griffies et al. 2000; Lee et al. 2002). This excessive diapycnal motion associated with the Veronis effect and numerical dispersion in the horizontal is not a feature of the eddy mass fluxes themselves but of the total mass flux featuring too large divergences. Integrations with and without EIT are subject to spurious diapycnal motion that arises from drift and numerics specific to level coordinate models. Most of this spurious diapycnal motion is rather small scale and of both signs. The result is that the net integrated diapycnal motion through any isopycnal is of realistic magnitude. However, the integrated absolute diapycnal motion through the same isopycnal may be too large by an order of magnitude! A particle that starts at one location with a certain density class and ends at another location within the same density class may on its way be subject to

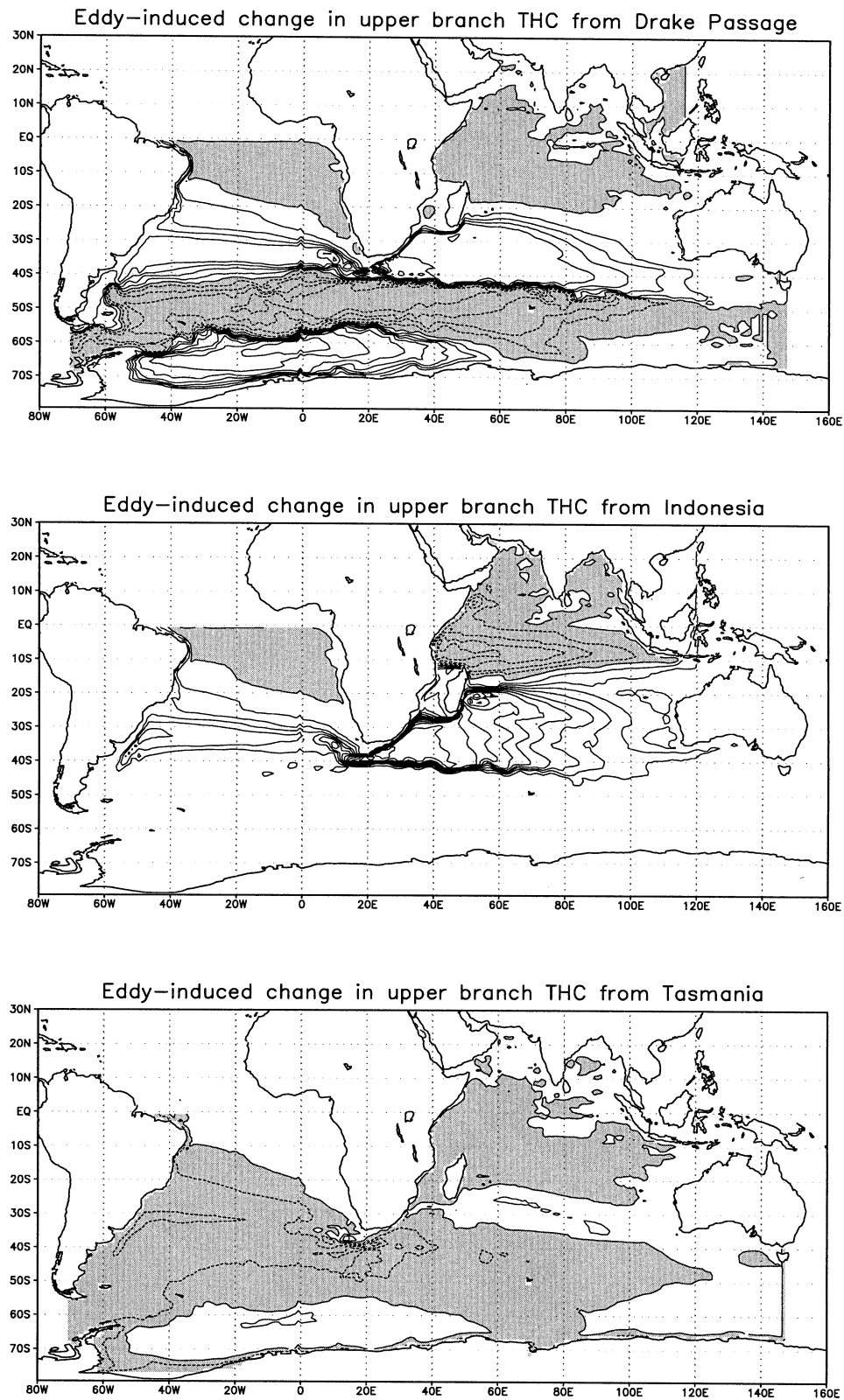


FIG. 2. Eddy-induced change in transport streamfunction of the upper branch of the THC for flow originating from Drake Passage, the Indonesian Throughflow, and the south of Australia. The contour interval is 0.5 Sv.

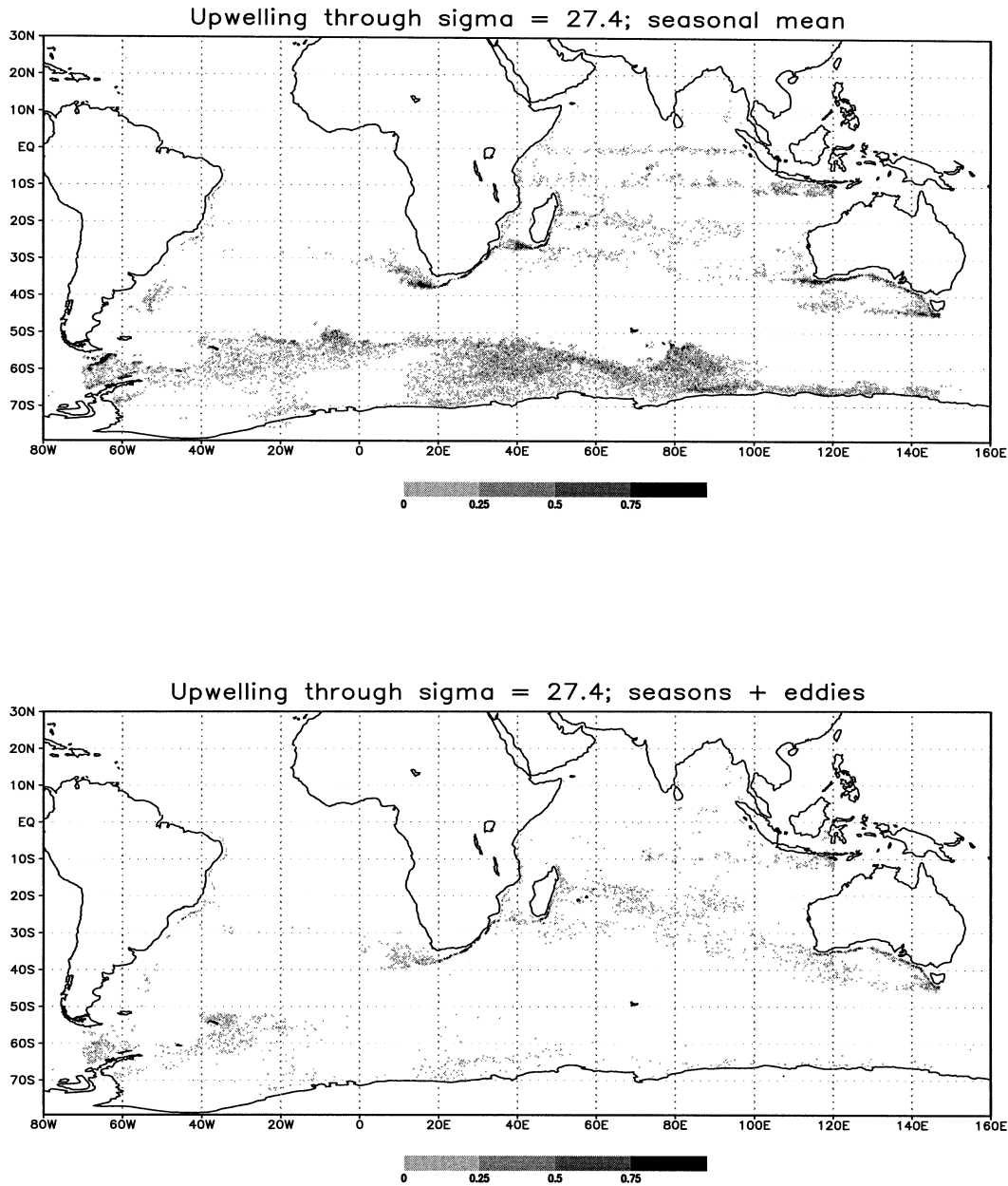


FIG. 3. Upward diapycnal transport through the $\sigma_0 = 27.4$ surface between the Indian–Atlantic borders and the Atlantic equator for the upper branch of the THC. With each particle a transport of about $250 \text{ m}^3 \text{ s}^{-1}$ is associated. Units are in $1000 \text{ m}^3 \text{ s}^{-1}$ per gridbox of $\frac{1}{4}^\circ$ by $\frac{1}{4}^\circ$. Total upwelling in the upper panel is 4.5 Sv; in the lower panel it is 1.0 Sv.

various upwelling and downwelling events across the level that bounds this density class. This problem is partly circumvented by considering only upwelling and downwelling from particles that start in one density class and end up in another. Still, the associated diapycnal motion is likely to be much too large in the model. The main point here is, however, that the ability of the EIT to counteract diapycnal motion associated with the divergences of the mean flow is large enough

to stand out against the noise of spurious diapycnal motion in the model.

4. Theoretical discussion

From Fig. 2 it may be seen that the main impact of the EIT on the upper branch of the THC is that circulations in the wind-driven gyres in closed basins are increased, while those in the Southern Ocean decrease.

Also, the eddy-induced changes do not just focus the flow in tight recirculations such as the Agulhas retroflexion, they have a major effect in the interior as well. Eddy-induced changes occur even where the eddy fluxes are weak! Where does the increase of circulation in the gyres come from? Increased circulation in a gyre means that the residence time of particles is increased; the circulation is prolonged. In general, particles can escape wind-driven circulations either from below where the influence of the wind forcing becomes negligible or from above where they can cross the boundaries by the Ekman flow. So, there are two processes by which the EIT can prolong the circulation in wind-driven gyres. First, by reducing diapycnal motion below the mixed layer. Second, by counteracting the Ekman flow within the mixed layer. The combined result of both processes may also lead to narrowing of the circulation patterns since a reduced transition probability will lead to sharper boundaries between circulation systems. This narrowing of circulation patterns can be inferred from Fig. 1. The reduction of diapycnal motion below the mixed layer was demonstrated in the former section. Below, we give some arguments why this occurs throughout the basin. Thereafter, we demonstrate that, within the mixed layer, the EIT counteracts the Ekman flow nearly everywhere in the basin and we discuss its implications.

a. Reduced diapycnal motion below the mixed layer

When the diabatic forcing is weak, a cancellation in buoyancy transport between eddies and mean flow occurs (Bryan 1986; Drijfhout 1994a). The reduction of diapycnal motion by the EIT can be understood from the same arguments. In isopycnic coordinates the time-averaged continuity equation reads (for steady state, $\partial \bar{h} / \partial t = 0$)

$$\nabla \cdot [\overline{\mathbf{u}(\sigma) \bar{h}(\sigma)}] + \nabla \cdot [\overline{\mathbf{u}'(\sigma) h'(\sigma)}] = \overline{F_Q(\sigma)}, \quad (2)$$

where F_Q represents diabatic effects. We define $\nabla \cdot [\overline{\mathbf{u}(\sigma) \bar{h}(\sigma)}] = \Delta \overline{w_{\text{mean}}(\sigma)}$, where w_{mean} is an apparent diapycnal velocity associated with mean flow divergences. Furthermore, we define $\nabla \cdot [\overline{\mathbf{u}'(\sigma) h'(\sigma)}] = \Delta \overline{w_{\text{eddy}}(\sigma)}$ and $\overline{F_Q(\sigma)} = \Delta \overline{w_{\text{diab}}(\sigma)}$, where $\overline{w_{\text{diab}}}$ is the true diapycnal velocity. Below the mixed layer, $\overline{w_{\text{diab}}}$ is almost everywhere small. Assuming zero diapycnal velocity at the bottom and integrating upward we have everywhere below the mixed layer:

$$\overline{w_{\text{mean}}} \gg \overline{w_{\text{diab}}} \quad \text{and} \quad (3)$$

$$\overline{w_{\text{mean}}} \approx -\overline{w_{\text{eddy}}}. \quad (4)$$

Just below the mixed layer w_{mean} is dominated by Ekman pumping and surface buoyancy forcing but may also include components due to friction, nonlinearities, and bottom topography. In a purely adiabatic ocean the balance of Eq. (4) holds exactly, also in the mixed layer. The Ekman overturning cells that appear in the streamfunction on z levels, representing the transport by the

mean flow only, disappear in the σ -coordinate representation of the streamfunction when the eddy transports have been included.

The inequality (3) means that the apparent diapycnal motion associated with mean flow divergences is much larger than the true diapycnal motion of the flow. Associated with the mean flow are vertical motions that do not correspond with any true watermass formation, or diapycnal motion. Inclusion of the EIT reduces the large apparent diapycnal motion of the mean flow to become the small true diapycnal motion. Equation (4) is a local balance that holds everywhere throughout the basin. This seems contradicted by the notion that eddy fluxes are associated with energetic currents and are smaller in the interior. The eddy fluxes, however, are dominated by the rotational fluxes (e.g., Drijfhout and Hazeleger 2001). The rotational fluxes locally enhance the tight recirculations in the very high energy zones near the boundaries. The much smaller divergent fluxes are associated with w_{eddy} . These fluxes hardly scale with the energy of the mean flow as they have to obey the balance of Eq. (4). Because the divergent eddy fluxes change the transition probability to go from one circulation to another, they are more important in changing the Lagrangian streamfunction than the rotational eddy fluxes.

b. Compensation of Ekman flow

The question whether the EIT in the mixed layer counteracts the Ekman flow can be rephrased as whether eddies play an important role in supplying the Ekman flows. This point has been advocated by a number of authors (e.g., Marshall et al. 1993; Tansley and Marshall 2001). It also underlies the representation of eddy effects in Gnanadesikan's (1999) model of the THC. Within the mixed layer Eq. (4) no longer holds because the diabatic forcing is nonnegligible. The discussion now focuses on the mass flux across a Bernoulli streamline because a local balance is no longer valid. From the time-averaged momentum equation and continuity equation a balance for the various mass fluxes across a time-averaged Bernoulli streamline can be derived. This balance boils down to transient eddy mass flux + Reynolds momentum flux + Ekman flux + frictional flux + diapycnal flux = 0 (Hallberg and Gnanadesikan 2001; Tansley and Marshall 2001).

In general, the Reynolds momentum flux is small; the frictional flux should become negligible when eddies are resolved but is sometimes still large in eddy-permitting models (Hallberg and Gnanadesikan 2001; Tansley and Marshall 2001). Tansley and Marshall (2001) studied this balance in a set of adiabatic runs and found a near cancellation between the Ekman flux and the transient eddy flux. Eddies supplied the Ekman flows completely. The integrated balance should hold locally as well because in an adiabatic ocean Eq. (4) is valid. Hallberg and Gnanadesikan (2001) studied the same bal-

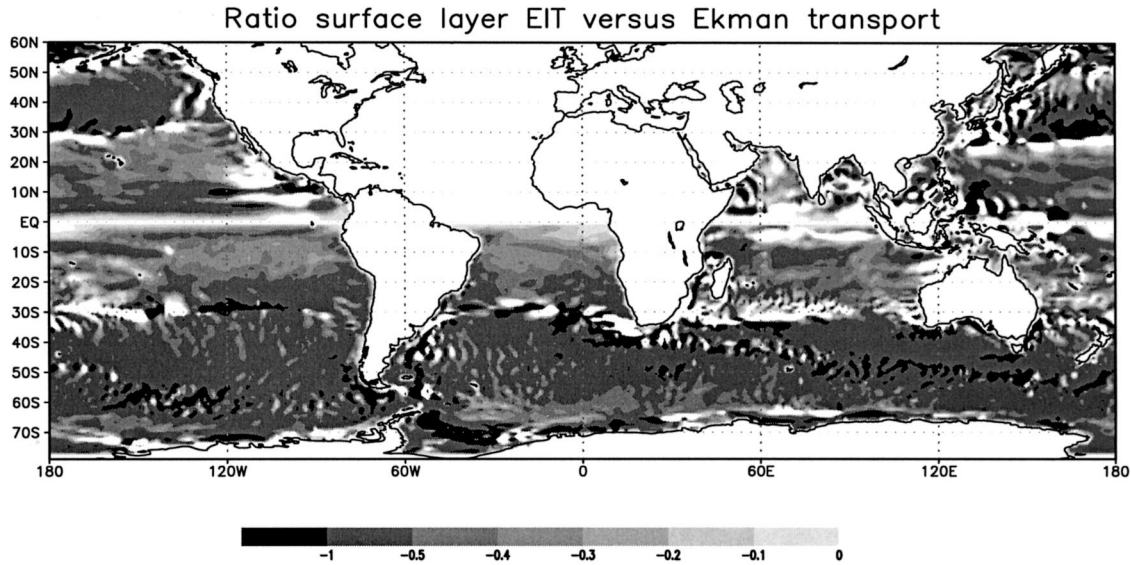


FIG. 4. Ratio of the surface layer EIT vs the Ekman transport. The ratio is calculated by projecting the upper-layer EIT vector onto the Ekman transport vector and by dividing by the squared magnitude of the Ekman transport; $(\mathbf{u}^* \cdot \mathbf{u}_{\text{Ek}})/\mathbf{u}_{\text{Ek}}^2$. The results are averaged for grid boxes of 1° by 1° . Results for the North Atlantic are not shown.

ance for a diabatically forced zonally reentrant channel flow with application to the ACC and found that in a realistic forcing regime the contribution of the transient eddy flux to the supply of the Ekman flux is significant. The extent to which eddies supply the Ekman flux now depends on the strength of the diabatic mass flux into the layer upstream of the Bernoulli streamline or inside that contour. This is determined by the strength of the diabatic forcing relative to the wind forcing. An appropriate scaling of the relative importance of the buoyancy forcing to the wind forcing was given in, for example, Drijfhout (1994b). It is measured by a nondimensional parameter Γ ,

$$\Gamma = L/(UT), \quad (5)$$

where L is the length scale of a wind-driven gyre, U is the wind-driven velocity, and T is the relaxation time for surface thermal anomalies. In general, the buoyancy forcing and wind forcing are of about equal strength. In this forcing regime, the transient eddy flux supplies a significant part of the Ekman flux in the Southern Ocean, according to Hallberg and Gnanadesikan (2001). For the EIT to have a systematic impact on the Lagrangian streamfunctions, the relevant questions are whether this supply is achieved locally or only comes about in an integrated sense and whether eddies also supply the Ekman flow outside the Southern Ocean.

To answer these questions we calculated the ratio of the component of the eddy flux parallel to the Ekman flux versus the magnitude of the Ekman flux: $(\mathbf{u}^* \cdot \mathbf{u}_{\text{Ek}})/\mathbf{u}_{\text{Ek}}^2$, in the uppermost layer for OCCAM (Fig. 4). Surprisingly, this ratio is almost uniformly negative. In general the eddies supply roughly 50% of the Ekman flux in OCCAM. Ratios are positive and/or not defined in

regions denoted by white areas. These are mainly found in the Tropics and regions where the wind stresses are weak, notably around 30°S and 30°N . Also some regions near the boundaries feature positive ratios. Outside the Tropics and the regions with weak winds the ratio is fairly uniform, slightly increasing with increasing latitude. So in the broad interior, the eddy mass flux counteracts the Ekman flux nearly everywhere. This result implies that with the EIT the ageostrophic component of the surface flow is counteracted and the flow occurs more along Bernoulli streamlines. Also, when the EIT is neglected, the wind-driven overturning cells are too strong and the supply of the Ekman flow involves too much diapycnal mixing and watermass formation.

5. Chaotic mixing

A fully deterministic velocity field that is associated with laminar advection may produce an essentially stochastic response in the Lagrangian advection characteristics of a passive tracer. Particle trajectories may separate exponentially in time and become chaotic. This flow, laminar from a dynamical point of view, displays Lagrangian turbulence from a kinematical viewpoint. The classical example of chaotic advection is Aref's (1984) problem in which it is shown that for 2D incompressible flow time dependence is sufficient to introduce chaotic advection. Chaotic mixing occurs whenever a streamfunction exhibits regions with closed streamlines separated by a temporal-fluctuating separatrix from regions with open streamlines. Large-scale horizontal mixing in 2D time-dependent flows with large vortical structures has been subject of a whole suite of meteorological studies (e.g., Pierrehumbert and

Yang 1993). In oceanography it has been applied to mixing in a meandering jet (e.g., Samelson 1992) and to the wind-driven double-gyre system (e.g., Liu and Yang 1994). In 3D flow a time-averaged streamfunction is obtained by integrating over one of the spatial coordinates. The streamlines of such a streamfunction reveal little of the properties of particle trajectories that are in most cases space filling. As a result, already very simple steady 3D flows may give rise to chaotic advection (e.g., Dombre et al. 1986). Chaotic mixing by steady 3D flows has not been studied a lot in geophysical fluid dynamics. One exception is the study of Yang and Liu (1997), who investigated the Lagrangian structure of an idealized wind-driven and buoyancy-driven circulation in a rectangular basin. In their case the forcing was steady and the flow became time independent after a spinup to equilibrium. They showed that the Lagrangian pathways and transport are chaotic and that there is a large-scale barrier to chaotic transport in the basin, which they call the “great ocean barrier.” Here, we investigate the Lagrangian structure of a more complex steady 3D flow.

In some experiments we have introduced a time dependence associated with the seasonal cycle, but this does not alter the Lagrangian structure of the flow considered nor does it increase significantly the chaotic mixing. The latter can be demonstrated from the dispersion of a cloud of particles. We calculated the zonal plus meridional variance of a particle cloud as a function of time. The cloud of 10 000 particles was initially located at the Atlantic equator, between 43.5° and 43.75°W and between depths of 778.82 and 915.12 m. The particles basically start in one grid box in the North Brazil Undercurrent (NBC) which carries the upper branch of the THC. The dispersion is qualitatively similar for cases with and without seasonal cycle and with and without the EIT. The largest exponential growth occurs in the first 3 months. If τ_2 is the time needed to double the sum of zonal and meridional variance $R^2(t)$, the finite-size Lagrangian Lyapunov exponent becomes (Artale et al. 1997)

$$\lambda_2 = \frac{\ln(2)}{\tau_2}, \quad (6)$$

where λ is the Lyapunov exponent. The Lyapunov exponent associated with advection by the time-independent annual mean flow with and without the EIT is about 20 day⁻¹ for the particle cloud discussed above. When time variability associated with the seasonal cycle is included the chaoticity increases and the Lyapunov exponent becomes 16 day⁻¹. So, the time-averaged flow under study exhibits chaos.

a. Lagrangian timescales

For each parcel the travel time, or time required when leaving one location (the Indian–Atlantic boundaries) to reach another location (the Atlantic equator), can be

calculated from the Lagrangian computations. Time histograms of these Lagrangian timescales and the time-integrated transport are presented in Fig. 5 for the water coming from Drake Passage. It is immediately evident that the distribution of travel time in both cases with and without the EIT is extremely skewed. The binned transport scales with the maximum of the integration with the EIT. In all cases the maximum transport is highest for the integration including the EIT. With the EIT, tail values are reduced and as a result the median transport time (T50%) is also reduced. Also, more transport is associated with the shortest timescales, less with the longest timescales, and peak values increase. In agreement with this, the relative difference in T90% (a factor of 4.7), is much larger than the relative difference in T50% (a factor of 2.1). A log–linear plot of the time-integrated transport (not shown) yields a straight line after year 400 for the integration including the EIT, which is associated with a tail that is approaching exponentially the limit value of 100%. The integration without the EIT does not show this behavior. Here, on longer timescales the functional dependency exhibits power-law behavior. As a result, with the EIT the mean value is well defined; without the EIT it is not. Apparently, the EIT significantly changes statistical aspects of the flow; the distribution of timescales and path length (not shown) is changed when the timescale becomes large. The same impact of the EIT on Lagrangian timescales occurs for the water originating from the Indonesian Throughflow and from south of Australia.

In Fig. 5 the yearly binned transport shows two large, distinct peaks for the case with the EIT. The first peak is associated with the direct route from Drake Passage, water recirculating (one time) in the subtropical gyre of the South Atlantic but not entering the Indian Ocean. The second peak is associated with water that recirculates one time in the South Atlantic–Indian supergyre. Both with and without the EIT the largest peak occurs at the same transport time (26 vs 28 yr). The peak associated with the direct route is absent when the velocities without the EIT are used. The increase in transport peak values at shorter timescales by the EIT and the reduction in transport time implies that more particles stay together on relatively fast direct routes. This is consistent with the observed focusing in strong (boundary) currents and gyre-scale recirculations by the EIT (Figs. 1 and 2). Back tracing, it is seen that particles, which at first are located in the NBC, disperse over three routes that end up at three different boundary sections of the Indian–Atlantic basin. This dispersion of particles at first close together (separated by a few kilometers) to different end sections many thousands of kilometers away from each other is due to the fundamental chaotic nature of the time-averaged 3D global THC (Yang and Liu 1997). The EIT cannot change this. It does, however, reduce the dispersion within each of these routes, which implies a decrease of chaotic mixing in the 3D thermohaline-driven flow. This is accomplished by con-

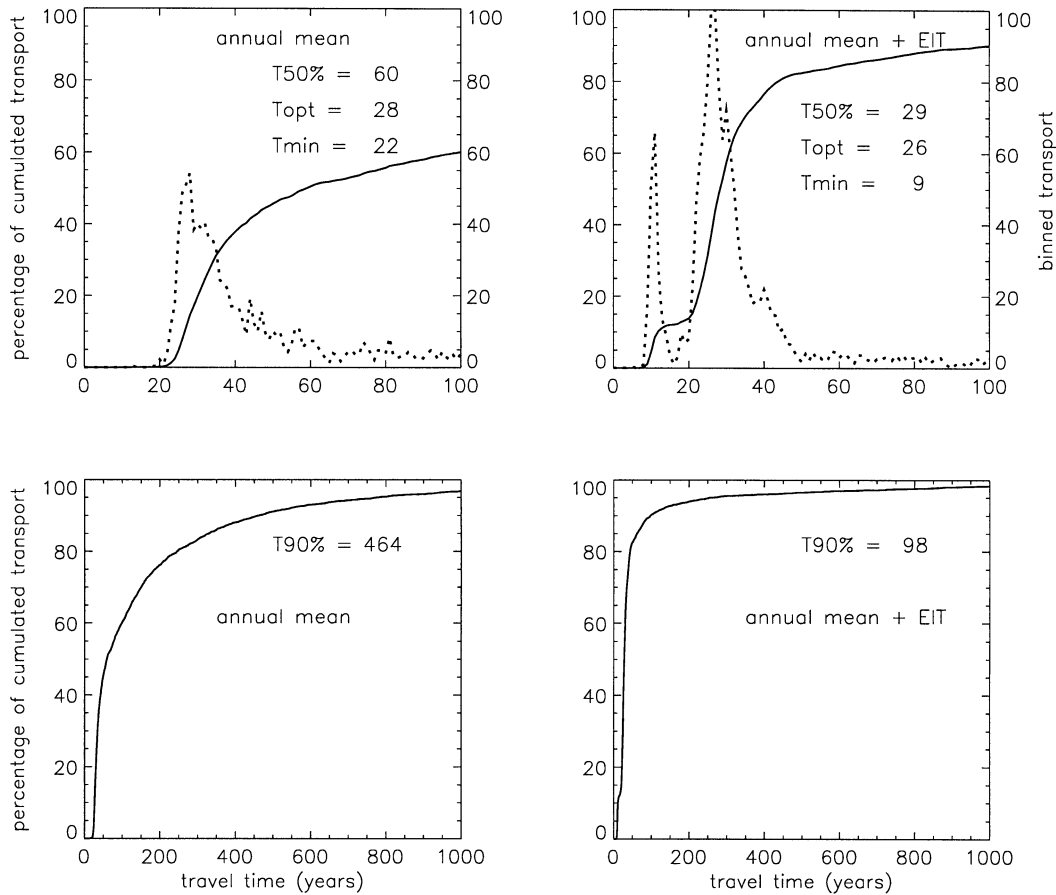


FIG. 5. Lagrangian timescale as a function of the yearly binned transport (dotted line) and the time-integrated transport in percentage of the total transport (solid line), for the upper branch of the THC with origins from Drake Passage. Left-hand panels denote the integration with annual mean velocities; right-hand panels the integration including the EIT. The yearly binned transport scales with the maximum of the integration including the EIT.

straining the flow more along isopycnals and reducing diapycnal motion. The EIT causes the flow to become more quasi 2D, although on the longer timescales and length scales the 3D aspect of the flow still cannot be neglected.

For back-traced particles that arrive at the boundary of the Indian–Atlantic basin within 50 years, particle spreading is dominated by advection in coherent circulation structures, see also Fig. 6. When particles are released at the Atlantic equator their initial positions are already structured according to the cross-equatorial northward transport; they are focused in the NBC. This feature of being a structured particle cloud survives apparently for 50 years or so. Without the EIT this feature is lost earlier. Particles with longer travel times exhibit more diffusive spreading. With the EIT there is a clear separation between the advective and diffusive spreading regimes. The advective regime is for fast travel times of less than 50 yr, the diffusive regime starts for travel times longer than 300 yr. In between is a transition regime. With the EIT the tail of the timescale distribution falls off exponentially. Without the EIT the ad-

vective and diffusive regimes are indistinguishable. Apparently, the spreading of particles and water masses without the EIT is governed by the “wrong” physics.

b. Particle distribution at the equator

When integrating particles backward from the Atlantic equator until they leave the Indian–Atlantic basin we can discriminate the particle distribution at the Atlantic equator with respect to origin (Drake Passage, Indonesian Throughflow, south of Tasmania). If the flow would be dominantly laminar, we would expect that the trajectories would be completely separated. When the flow is more chaotic, the trajectories will become more and more mixed. To illustrate in yet another way that the EIT tends to decrease chaotic mixing we compare results from the integration with annual mean fields with and without the EIT. Figure 7 singles out the western boundary region from 44° to 43° W, which contains about 80% of the trajectories in each case. In both cases trajectories in the upper 400 m are distributed randomly with respect to origin, suggesting complete chaotic mix-

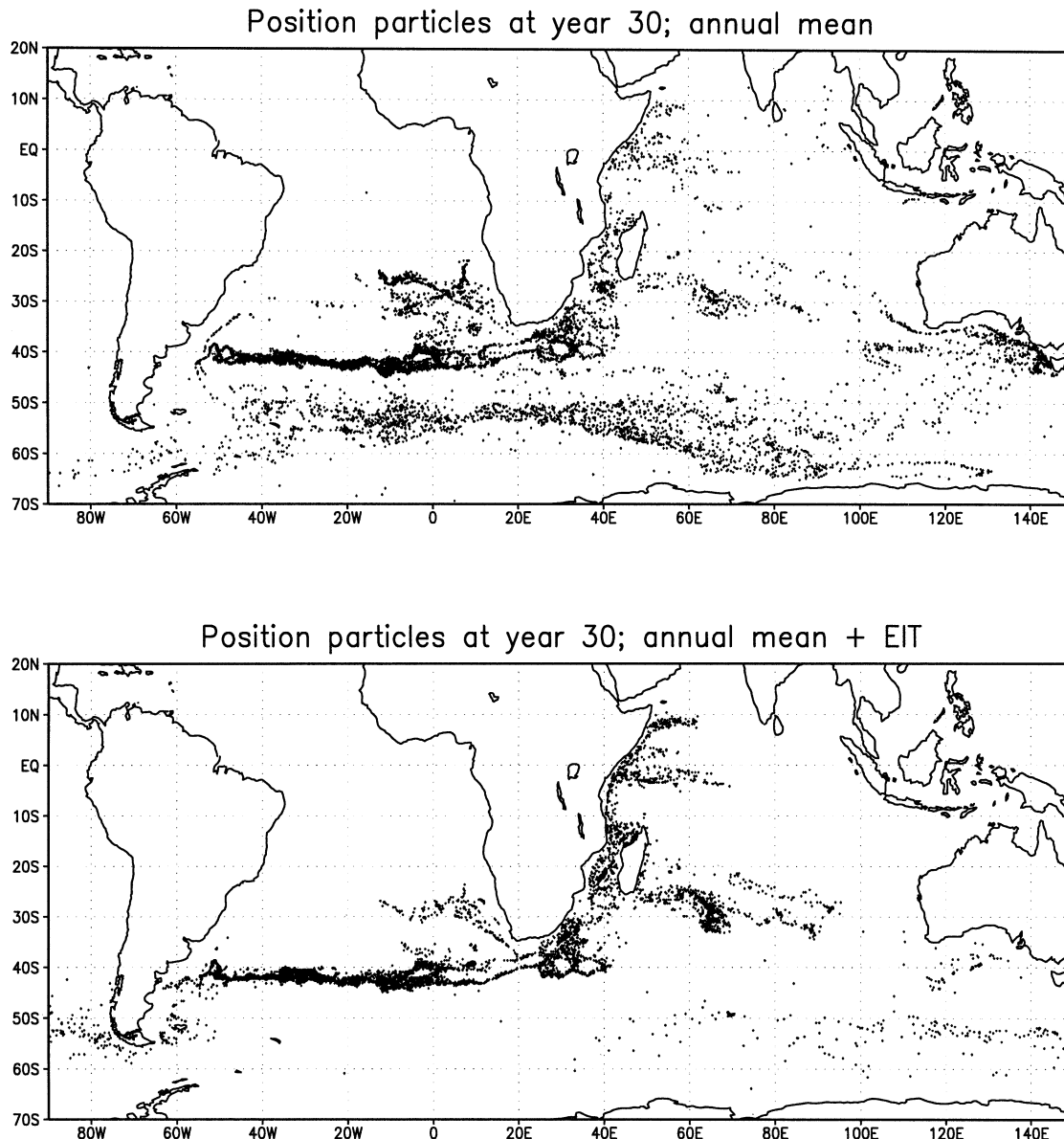


FIG. 6. Maps showing the dispersion of a cloud of back-traced particles after 30 yr, that eventually leave, or have left, the Indian–Atlantic basin through Drake Passage. The particles are initially localized at the Atlantic equator between 43.5° and 43.75°W and depths of 778.82 and 915.12 m. Shown are cases with and without the EIT. The integration shown here does not stop at the Indian–Atlantic boundaries. We have singled out the region where most particles are found.

ing (not shown). Largest differences appear beneath 400 m. The interval shown, from 400 to 900 m, contains 25%–30% of the trajectories. There is a relative abundance of trajectories from the south of Tasmania, flowing deeper, and a relative shortage of those from the Indonesian Throughflow, which occupy shallower positions. This separation in the vertical is more prominent with the EIT than without. In the case without the EIT the distribution remains random; with the EIT the distribution is more regular with most trajectories from Drake Passage close to the boundary and most trajec-

tories from the Indonesian Throughflow at the eastern flank of the NBC. The middle is dominated by trajectories from the south of Tasmania.

Yang and Liu (1997) conjecture that the chaotic nature of the time-averaged flow arises from the combination of a buoyancy-driven flow in the meridional plane and wind-driven motion in the horizontal plane. With a realistic geometry and bottom topography the buoyancy-driven flow itself is probably chaotic when it becomes 3D. The purely wind-driven flow still may be regular as it is constrained to flow along isopycnals.

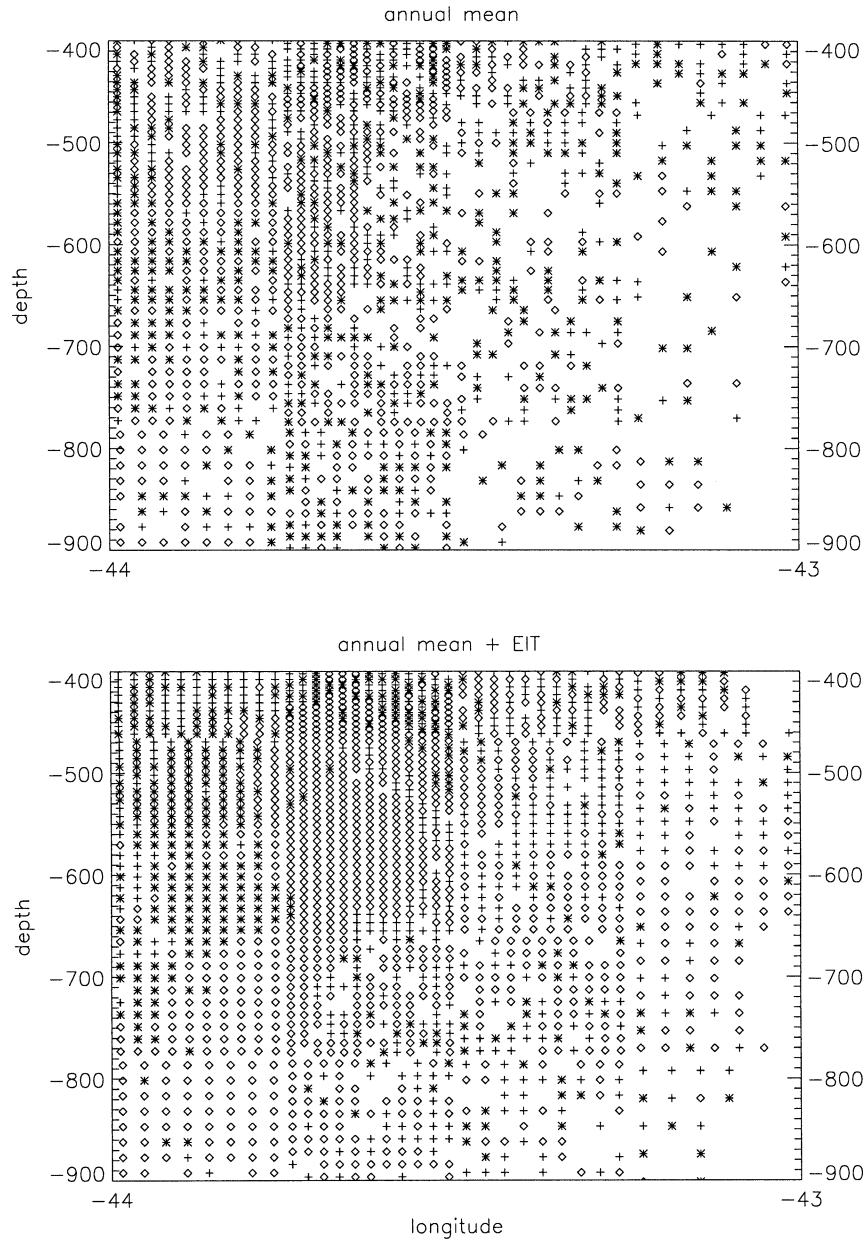


FIG. 7. Cross section of the upper branch of the THC at the Atlantic equator showing trajectories from Drake Passage (asterisks), the Indonesian Throughflow (plus signs), and the south of Australia (diamonds). With each particle a transport of about $2500 \text{ m}^3 \text{ s}^{-1}$ is associated. The lower panel shows results with the EIT, the upper panel shows them without the EIT. In the upper panel, symbols are mixed everywhere. The lower panel shows a sense of order by distinct regions in which all the symbols are the same.

Thus, diapycnal motions make the flow chaotic. Because the flow without EIT contains more diapycnal motion than the flow with EIT, the latter is less chaotic. It should be emphasized that the time variability associated with the eddy field itself (which we have excluded in these integrations) will have the opposite effect on the flow as the EIT does and will increase dispersion and chaotic mixing. If we would be able to

resolve the full time-dependent motion of the eddy field, the flow could become either more or less chaotic due to eddies, depending on which effect would be stronger: the increase of dispersion associated with stochastic turbulent motion or the decrease of dispersion due to reduced diapycnal motion. It is interesting to note that results from simple kinematic models of strong, meandering jets that include time dependence

(e.g., Samelson 1992) suggest that the flow in the core of strong currents remains focused and is not easily mixed with the surroundings.

6. Summary and conclusions

The impact of the eddy-induced transport (EIT) on the Lagrangian structure of the upper branch of the THC has been investigated. To this end, the OCCAM global eddy-permitting ocean model was used with horizontal resolution of $\frac{1}{4}^\circ$ by $\frac{1}{4}^\circ$. The Lagrangian pathways, transports, and mixing characteristics were diagnosed employing Lagrangian trajectories.

In all aspects of the flow investigated the neglect of the EIT leads to severely biased results. It is found that the EIT focuses the flow in (western) boundary currents. Recirculation in the wind-driven gyres increases. The EIT does not act as diffusion but as upgradient momentum transfer where western boundary currents and tight recirculations in wind-driven gyres are present. It decreases wide (supergyre) recirculations. The inclusion of EIT prolongs circulation in wind-driven gyres and reduces the transition probability to go from one circulation to another. One reason is that EIT reduces diapycnal motion that moves particles upward or downward in wind-driven gyres until they escape the circulation from below or from above by the Ekman flow. Below the mixed layer the divergences of the eddy mass fluxes nearly cancel those of the mean flow. In the surface mixed layer, the EIT counteracts the Ekman flow. This compensation occurs locally and is found throughout the basin. Typically, the surface layer EIT reduces the Ekman transport by 50%.

The time-averaged THC features chaotic mixing due to its three-dimensionality. The EIT decreases diapycnal motion, which makes the flow more shallow and aligned along isopycnals. As a result, the EIT reduces chaotic mixing. Particle distributions show less spread and the distribution of transport times becomes more peaked. This is most noticeable for intermediate waters (the densest classes of the upper branch of the THC), and for flow from Drake Passage. Without the EIT the advective and diffusive regimes of the particle spreading are indistinguishable. The statistical aspects of the flow are significantly changed by the EIT as reflected by a different time dependence of the distribution of the flow in Lagrangian transport time and path length. The spreading of particles and water masses without the EIT is governed by the “wrong” physics. These results imply that EIT parameterizations (when acting in the same way as the EIT does in eddy-permitting and eddy-resolving models) will improve the representation of western boundary currents and wind-driven recirculations, which are badly resolved in coarse-resolution ocean models. Also, a parameterized EIT will counteract the climate drift that arises from the spurious diapycnal motion and implied watermass conversion that is associated

with the Eulerian mean flow resulting from the observed large-scale density distribution in the ocean.

Acknowledgments. This work was supported by the MASTIII project TRACMASS (Contract MAS3-CT97/0142), funded by the European Community.

REFERENCES

- Aref, H., 1984: Stirring by chaotic advection. *J. Fluid Mech.*, **143**, 1–21.
- Artale, V., G. Boffetta, A. Celani, M. Cencini, and A. Vulpiani, 1997: Dispersion of passive tracers in closed basins: Beyond the diffusion coefficient. *Phys. Fluids*, **9**, 3162–3171.
- Blanke, B., and S. Raynaud, 1997: Kinematics of the Pacific Equatorial Undercurrent: An Eulerian and Lagrangian approach from GCM results. *J. Phys. Oceanogr.*, **27**, 1038–1053.
- Bryan, K., 1986: Poleward buoyancy transport in the ocean and mesoscale eddies. *J. Phys. Oceanogr.*, **16**, 927–933.
- Danabasoglu, G., and J. C. McWilliams, 1995: Sensitivity of the global ocean circulation to parameterizations of mesoscale tracer transports. *J. Climate*, **8**, 2967–2987.
- de Ruijter, W. P. M., 1982: Asymptotic analysis of the Agulhas and Brazil Current systems. *J. Phys. Oceanogr.*, **12**, 361–373.
- de Vries, P., and K. Döös, 2001: Calculating Lagrangian trajectories using time-dependent velocity fields. *J. Atmos. Oceanic Technol.*, **18**, 1092–1101.
- Dombre, T., U. Frisch, J. M. Greene, M. Hénon, A. Mehr, and A. M. Soward, 1986: Chaotic streamlines in the ABC flows. *J. Fluid Mech.*, **167**, 353–391.
- Döös, K., 1995: Inter-ocean exchange of water masses. *J. Geophys. Res.*, **100**, 13 499–13 514.
- , and D. J. Webb, 1994: The Deacon cell and other meridional cells of the Southern Ocean. *J. Phys. Oceanogr.*, **24**, 429–442.
- , and A. C. Coward, 1997: The Southern Ocean as the major upwelling zone of North Atlantic Deep Water. *International WOCE Newsletter*, No. 27, WOCE International Project Office, Southampton, United Kingdom, 3–4.
- Drijfhout, S. S., 1994a: On the heat transport by mesoscale eddies in an ocean circulation model. *J. Phys. Oceanogr.*, **24**, 353–369.
- , 1994b: Sensitivity of eddy-induced heat transport to diabatic forcing. *J. Geophys. Res.*, **99**, 18 481–18 499.
- , and W. Hazeleger, 2001: Eddy mixing of potential vorticity versus thickness in an isopycnal ocean model. *J. Phys. Oceanogr.*, **31**, 481–505.
- , E. Maier-Reimer, and U. Mikolajewicz, 1996: Tracing the conveyor belt in the Hamburg large-scale geostrophic ocean general circulation model. *J. Geophys. Res.*, **101**, 22 563–22 575.
- England, M. H., 1993: Representing the global-scale water masses in ocean general circulation models. *J. Phys. Oceanogr.*, **23**, 1523–1552.
- Gent, P. R., and J. C. McWilliams, 1990: Isopycnal mixing in ocean circulation models. *J. Phys. Oceanogr.*, **20**, 150–155.
- Gnanadesikan, A., 1999: A simple predictive model for the structure of the oceanic pycnocline. *Science*, **283**, 2077–2079.
- Griffies, S. M., R. C. Pacanowski, and R. W. Hallberg, 2000: Spurious diapycnal mixing associated with advection in a z -coordinate ocean model. *Mon. Wea. Rev.*, **128**, 538–564.
- Hallberg, R. W., and A. Gnanadesikan, 2001: An exploration of the role of transient eddies in determining the transport of a zonally reentrant current. *J. Phys. Oceanogr.*, **31**, 3312–3330.
- Hazeleger, W., P. de Vries, and G. J. van Oldenborgh, 2001: Do tropical cells ventilate the Indo-Pacific equatorial thermocline? *Geophys. Res. Lett.*, **28**, 1763–1766.
- , —, and Y. Friocourt, 2003: Sources of the Equatorial Undercurrent in the Atlantic in a high-resolution ocean model. *J. Phys. Oceanogr.*, **33**, 677–693.
- Hirst, A. C., and T. J. McDougall, 1998: Meridional overturning and

- dianeutral transport in a z -coordinate ocean model including eddy-induced advection. *J. Phys. Oceanogr.*, **28**, 1205–1223.
- Killworth, P. D., 1996: Time interpolation of forcing fields in ocean models. *J. Phys. Oceanogr.*, **26**, 136–143.
- Lee, M.-M., A. C. Coward, and A. J. G. Nurser, 2002: Spurious diapycnal mixing of the deep waters in an eddy-permitting global ocean model. *J. Phys. Oceanogr.*, **32**, 1522–1535.
- Liu, Z., and H. Yang, 1994: The intergyre chaotic transport. *J. Phys. Oceanogr.*, **24**, 1768–1782.
- Marshall, J., D. Olbers, H. Ross, and D. Wolf-Gladrow, 1993: Potential vorticity constraints on the dynamics and hydrography of the Southern Ocean. *J. Phys. Oceanogr.*, **23**, 465–487.
- McDonald, A. M., and C. Wunsch, 1996: An estimate of global ocean circulation and heat fluxes. *Nature*, **382**, 436–439.
- Nycander, J., K. Döös, and A. C. Coward, 2002: Chaotic and regular trajectories in the Antarctic Circumpolar Current. *Tellus*, **54**, 99–106.
- Pierrehumbert, R. T., and H. Yang, 1993: Global chaotic mixing on isentropic surfaces. *J. Atmos. Sci.*, **50**, 2462–2480.
- Samelson, R. M., 1992: Fluid exchange across a meandering jet. *J. Phys. Oceanogr.*, **22**, 431–440.
- Saunders, P. M., A. C. Coward, and B. A. de Cuevas, 1999: Circulation in the Pacific Ocean seen in a global ocean model: Ocean Circulation and Climate Advanced Modelling project (OCCAM). *J. Geophys. Res.*, **104**, 18 281–18 299.
- Semtner, A. J., and R. C. Chervin, 1992: Ocean general circulation from a global eddy-resolving model. *J. Geophys. Res.*, **97**, 5493–5550.
- Speich, S., B. Blanke, and G. Madec, 2001: Warm and cold water routes of an OGCM thermohaline conveyor belt. *Geophys. Res. Lett.*, **28**, 311–314.
- , —, P. de Vries, K. Döös, S. S. Drijfhout, A. Ganachaud, and R. Marsh, 2002: Tasman leakage: A new route in the global ocean conveyor belt. *Geophys. Res. Lett.*, **29**, 1416, doi:10.1029/2001GL014586.
- Tansley, C. E., and D. P. Marshall, 2001: On the dynamics of wind-driven circumpolar currents. *J. Phys. Oceanogr.*, **31**, 3258–3273.
- Thompson, S. R., D. P. Stevens, and K. Döös, 1997: The importance of interocean exchange south of Africa in a numerical model. *J. Geophys. Res.*, **102**, 3303–3315.
- Toggweiler, J. R., and B. Samuels, 1995: Effect of Drake Passage on the global thermohaline circulation. *Deep-Sea Res.*, **42**, 477–500.
- Webb, D. J., A. C. Coward, B. A. de Cuevas, and C. S. Gwilliam, 1997: A multiprocessor ocean general circulation model using message passing. *J. Atmos. Oceanic Technol.*, **14**, 175–183.
- Yang, H., and Z. Liu, 1997: The three-dimensional chaotic transport and the great ocean barrier. *J. Phys. Oceanogr.*, **27**, 1258–1273.